[6] V. I. Veksler et al., Proc. VIth Int. Conf. on High-Energy Accelerators (Cambridge Electron Accelerator Report No. CEAL-2000) 1967, p. 289.
[7] A. Schlüter, Proc. VIIIth Int. Conf. on High-Energy Accelerators, CERN, Geneva 1971, p. 402.
[8] U. Schumacher, in Collective Ion Acceleration, Springer Tracts in Modern Physics, Vol. 84, Springer-Verlag, Berlin 1979.
[9] U. Schumacher, C. Andelfinger, and M. Ulrich, Phys. Letters **51 A**, 367 (1975).
[10] G. V. Dolbilov et al., Proc. Third Int. Conf. on Collective Methods of Acceleration, Irvine (USA), p. 83, Harwood Acad. Publ., New York 1979.
[11] W. B. Lewis, Proc. Symp. on Electron Ring Accelerators, Lawrence Radiation Laboratory, Berkeley, California, USA, Report UCRL-1803 (1968).
[12] G. I. Budker, Atomnaya Energiya **1**, 9 (1956).
[13] R. P. Godwin, Springer Tracts in Mod. Physics **51** (1969); C. Kunz (ed.): Synchrotron Radiation, Techniques and Applications (Topics in Current Physics, Vol. 10), Springer-Verlag, Berlin 1979.
[14] I. Boscolo et al., IEEE Trans. Nucl. Sci. **NS-19**, **2**, 287 (1972) and Proc. 2nd Int. Conf. on Ion Sources, Vienna 1972, p. 654.
[15] G. Brautti et al., IEEE Trans. Nucl. Sci. **NS-20**, **3**, 286 (1973).

Selfsimilar Spherical Compression Waves in Gas Dynamics *

J. Meyer-ter-Vehn and C. Schalk
Max-Planck-Institut für Quantenoptik, Garching

Z. Naturforsch. **37a**, 955–969 (1982); received May 28, 1982

To Professor Arnulf Schlüter on his 60th Birthday

A synopsis of different selfsimilar spherical compression waves is given pointing out their fundamental importance for the gas dynamics of inertial confinement fusion. Strong blast waves, various forms of isentropic compression waves, imploding shock waves and the solution for non-isentropic collapsing hollow spheres are included. A classification is given in terms of six singular points which characterise the different solutions and the relations between them. The presentation closely follows Guderley's original work on imploding shock waves.

1. Introduction

It is now 40 years ago that Guderley's pioneering paper on spherical imploding shock waves appeared [1]. The outstanding importance of this paper is not just that it solved the particular problem in an elegant way, but it opened the view to a much broader class of selfsimilar solutions in gas dynamics. Guderley discussed the general pattern of these solutions, but time was premature then for a detailed assessment of each individual branch. Now over the last 10 years, research on inertial confinement fusion (ICF) has triggered specific new interest in this problem. The concept of spherical implosion of small target spheres [2] leading to very high compression ($\cong 10^3$ times solid density) and high temperatures (ignition temperature of DT fuel $\geqq 5$ keV) exploits the singular behaviour of spherically imploding waves near the center, and selfsimilar waves represent a basic approach to the gas-dynamical part of the problem. Several papers on isentropic selfsimilar compression to high densities have been published. In particular, Kidder's analytical solution for homogeneous compression [3] has played a considerable role in clarifying general features of the process. Its derivation in Lagrangian coodinates as given by Kidder is remarkably simple, but leaves the relation to other selfsimilar waves obscure.

It is the intention of this paper to show the generic relations between the different isentropic and non-isentropic selfsimilar waves, imploding and exploding, by placing all of them on Guderley's original chart of solutions. This will include the cumulative isentropic solutions of Kidder [3, 4] and Anisimov et al. [5], where all matter finally collapses into a point, the non-cumulative isentropic solutions discussed by Ferro Fontan et al. [6] and Rodriguez et al. [7], which contain the reflected shock after the imploding wave has reached the centre, and finally the imploding shock solution [1] and its extension to non-isentropic imploding shells. The latter is closest to the situation in ICF target implosions, and it will be shown that the solution in the centre behind the reflected shock after shell collapse, where DT ignition and burn has to be achieved in fusion applications, is of the same origin as the famous blast wave solution of Taylor [8] and Sedov [9].

Let us make some further remarks on the history of the problem and add some references. According to Zeldovich [10] the imploding shock solution has been found independently of Guderley's work also by Landau and Stanyukovich around 1945, and Russian physicists and mathematicians have been most active in the study of selfsimilar motion in the following time. The books of Sedov [11] (1959), Stanyukovich [12] (1960), Zeldovich and Raizer [10] (1967), and the recent one of Barenblatt [13] (1979) give broad access to this work. An early account of spherical selfsimilar waves is also given in the book of Courant and Friedrichs [14] (1948). An extension of Guderley's work to plane shock waves has been investigated by Weizsäcker [15] (1954), Häfele [16, 17] (1955) and others [18, 19]. The important problem of impulsive load on a plane surface has been thoroughly discussed by Zeldovich (1956, see Ref. [10]). Propagation of a

* This work was supported by the Bundesministerium für Forschung und Technologie and Euratom.

Reprint requests to Dr. Meyer-ter-Vehn, Max-Planck-Institut für Quantenoptik, D-8046 Garching.

0340-4811 / 82 / 0800-0955 $ 01.30/0. — Please order a reprint rather than making your own copy.

plane shock in a medium with decreasing density (power law distribution) has been treated by Sakurai [20] (1960). The problem of a collapsing bubble turned out to be of Guderley's type as shown by Hunter [21] (1960). Several authors have determined the selfsimilarity exponent of the imploding shock as a function of the specific heat ratio γ by approximate methods [22 – 24] and numerical calculations [25, 26]. A rather detailed study of the different γ regions for shock and bubble implosions has been performed by Brushlinski and Kazhdan [27] (1963). The linear stability of various selfsimilar spherical waves with respect to spherically asymmetric perturbations (e. g. Rayleigh-Taylor instability) has been investigated recently, in particular by Kidder [4], Bernstein and Book [28 – 30], and by Brushlinski [31]. An assessment of this work would be beyond the scope of this paper.

A further comment is made on the general nature of selfsimilar solutions. It has been emphasized by Barenblatt [13] that these solutions are more than just incidental particular solutions which happen to be simple, but that they represent important asymptotic solutions in a certain sense which Barenblatt calls "intermediate asymptotics". In the case of Guderley's shock solution this implies that a large class of non-selfsimilar spherically imploding waves with rather general boundary conditions outside and a shock front propagating into unperturbed gas at the inner boundary approaches the selfsimilar solution asymptotically for radii r and times t close enough to the collapse point $r=0$ and $t=0$. On the other hand, shock velocity and strength as well as temperature behind the front and other quantities are diverging upon spherical convergence in Guderley's solution. This is certainly an unphysical behaviour and will be limited e. g. by heat conduction, radiation and other processes which are neglected in pure gas dynamics as considered here. For this reason real shock implosions will deviate from the selfsimilar solution also in the centre and a small region surrounding it. It is therefore typically an intermediate region where the selfsimilar solution is approached by more realistic, non-selfsimilar solutions and this leads to the term "intermediate asymptotics". In most cases it is very difficult to determine the regions of intermediate asymptotics in a general way since usually nothing general is known about the larger class of non-selfsimilar solutions. A remarkable attempt to gain some general insight in non-selfsimilar flow neighbouring selfsimilar flow in Guderley's problem has been made by Häfele [17]. But otherwise only numerical results based on finite difference schemes exist for comparisons. They have been studied extensively for ICF target implosions. It is interesting to see that salient features of such numerical implosion calculations are indeed well reproduced by selfsimilar solutions, and the concept of intermediate asymptotics appears to be useful, although no precise statements can be made so far. More work has to be done to establish the regions of intermediate asymptotics for spherical implosions more precisely.

In the following the different branches of selfsimilar solutions which may be approached in ICF target calculations are discussed. Although the basic equations have been derived at a number of places (see e. g. Refs. [1, 10 – 12, 14]), a brief derivation is repeated in Sect. 2 and the appendix. A new aspect is found in Sect. 2.2 by taking into account particle trajectories explicitly; this leads to a general theorem concerning ratios of density, pressure etc. on such trajectories. Algebraic integrals expressing mass and entropy conservation are derived in Section 2.3. The reduced differential equation is obtained in Section 2.4. Singular points and boundary conditions are discussed in Section 2.5. The particular solutions shown in the figures of the following sections have been obtained by numerical integration of the reduced equations in those cases where no analytic solution exists.

2. The Basic Equations and Guderley's General Solution

2.1. *The Gasdynamical Equations and the Selfsimilarity Ansatz*

The basic gasdynamical equations

$$\begin{aligned} &\partial/\partial t\,\varrho + \partial/\partial r(\varrho u) + (n-1)\,\varrho u/r = 0\,, \\ &\partial/\partial t\,u + u(\partial/\partial r)u + (1/\varrho)(\partial/\partial r)p = 0\,, \\ &\partial/\partial t(p/\varrho^{\gamma}) + u(\partial/\partial r)(p/\varrho^{\gamma}) = 0 \end{aligned} \tag{1}$$

express conservation of mass, momentum and entropy. They are given here for plane ($n=1$), cylindrical ($n=2$) or spherical ($n=3$) symmetry with a single spatial coordinate r. The entropy function $A=p/\varrho^{\gamma}$ is chosen for an ideal gas with the adiabatic exponent γ. For selfsimilar solutions

the equations of gas dynamics (1) reduce to a single ordinary differential equation. The selfsimilarity ansatz for the density $\varrho(r,t)$, the velocity $u(r,t)$ and the sound velocity $c(r,t)$ (defined by $c^2 = \gamma p/\varrho$) is chosen in the form

$$u(r,t) = (\alpha r/t)\,U(\xi),$$
$$c(r,t) = (\alpha r/t)\,C(\xi), \qquad (2)$$
$$\varrho(r,t) = (r^{\varkappa})\,G(\xi),$$

where the selfsimilarity coordinate is defined as

$$\xi = r/|t|^{\alpha}. \qquad (3)$$

The selfsimilarity exponent α and the density exponent $\varkappa$ are free parameters. It is assumed that radius r and time t are measured in units r_0 and t_0, and velocities in units r_0/t_0. For singular waves like an imploding spherical shock wave converging to a point $r=0$ at $t=0$ or an outgoing shock emerging from $r=0$ at $t=0$ in a point explosion, the ansatz (2) and (3) is very useful since the shock front moves on a line of constant ξ under certain conditions. These are the selfsimilar waves considered in this paper. For example, the shock front of a strong point explosion in a uniform gas travels along $R_s = \xi_s t^{2/5}$ where the selfsimilarity exponent $\alpha = 2/5$ follows from simple dimensional analysis in this case. For illustration, lines of constant ξ in the r,t plane have been plotted in Figure 1. The ξ lines emerge from $r=0$, $t=0$ symmetrically for $t<0$ and $t>0$; the time axis $r=0$ corresponds to $\xi=0$ and the radial axis $t=0$ to $\xi=\infty$. Material boundaries such as a surface and characteristics may coincide with ξ lines as well as shock fronts. This is discussed in the next section.

Here, we add a remark on the special form of ansatz (2) for $t=0$ and a list of notations. At time $t=0$, the variables of selfsimilar flow obey simple power laws

$$u(r,t=0) = u_0\, r^{-\lambda}, \quad c(r,t=0) = c_0\, r^{-\lambda},$$
$$\varrho(r,t=0) = \varrho_0\, r^{\varkappa}, \quad p(r,t=0) = p_0\, r^{\varkappa-2\lambda},$$
$$A(r,t=0) = p/\varrho^{\gamma} = A_0\, r^{-\varepsilon} \qquad (4)$$

provided that the limits for $t \to 0$ exist. The constants are obtained from (2) with $|t| = (r/\xi)^{1/\alpha}$ in the limit $\xi \to \infty$. Combinations of the basic parameters n, γ, α, $\varkappa$ appearing in (4) and throughout the paper are listed here, for reference:

$$\lambda = 1/\alpha - 1, \quad \varepsilon = \varkappa(\gamma-1) + 2\lambda, \qquad (5)$$
$$\mu = 2/(\gamma-1), \quad \beta = n - \mu\lambda, \quad \nu = n\gamma + \varkappa - 2\lambda.$$

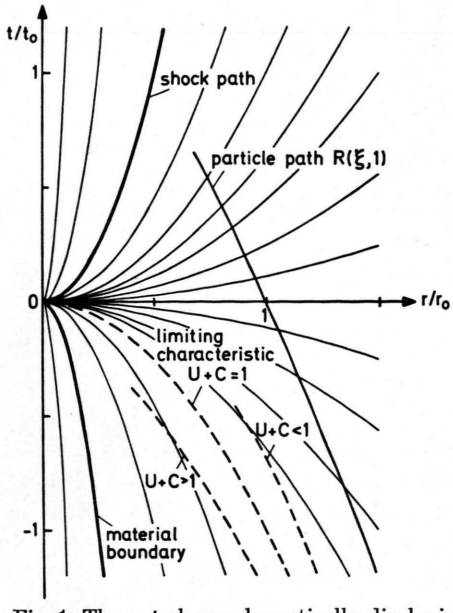

Fig. 1. The r, t plane schematically displaying various important curves. The thin solid curves are lines on which the selfsimilarity coordinate $\xi = r/|t|^{\alpha}$ is constant. The exponent $\alpha = 1/2$ has been chosen. In some important cases, ξ lines coincide with material boundaries, shock paths or characteristics. A particle trajectory $R(\xi, 1)$ is also shown.

Isentropic flow occurs for $\varepsilon = 0$. Also note from (4) that selfsimilar flow is characterised by uniform Mach number $M_0 = u_0/c_0$ at $t=0$.

2.2. *Particle Trajectories and Characteristics*

Before discussing the reduced equations, some important relations are derived which are a direct consequence of the selfsimilarity ansatz itself. Let us introduce trajectories $R(t,a)$ of gas elements where the Lagrangian coordinate $a = R(t_0, a)$ labels each element by its position at a suitable time t_0. Combining the equation for R

$$\mathrm{d}R/\mathrm{d}t = u(R,t)$$

with the selfsimilar form (2) for $u(r,t)$, one finds after some algebra

$$\mathrm{d}\ln R(\xi,a)/\mathrm{d}\ln\xi = U(\xi)/(U(\xi)-1), \qquad (6)$$

where $R(\xi,a)$ is now interpreted as a function of ξ and time follows from $|t(\xi,a)| = (R/\xi)^{1/\alpha}$. An illustrative example of a particle path is shown in Figure 1. From (6) it follows immediately that

$$U = 1 \qquad (7)$$

is the condition for a trajectory to coincide with a ξ line. Selfsimilar motion of a free surface is there-

fore described by $U=1$. Another important consequence of (6) follows from the fact that its right side does not depend on a:

$$R(\xi_1, a_1)/R(\xi_2, a_1) = R(\xi_1, a_2)/R(\xi_2, a_2) \quad (8)$$

(arbitrary $\xi_{1,2}, a_{1,2}$).

The ratio of positions $R(\xi, a_1)$ of a particle a_1 on different ξ lines ξ_1 and ξ_2 is the same as for particle a_2 or any particle. Proportions of form (8) hold also for the particle's density

$$\varrho(\xi_1, a_1)/\varrho(\xi_2, a_1) = \varrho(\xi_1, a_2)/\varrho(\xi_2, a_2) \quad (9)$$

and all other state variables like pressure p, temperature T etc. where $\varrho(\xi, a) := \varrho(R(\xi, a), t(\xi, a))$, etc. This is obtained from combining relations (2) and (8). These general proportions are very helpful for discussing properties of particular solutions in the following.

Characteristics $R^{\pm}(t, a)$ are defined by

$$\mathrm{d}R^{\pm}/\mathrm{d}t = u(R^{\pm}, t) \pm c(R^{\pm}, t). \quad (10)$$

Applying the same transformations as to (6), one obtains

$$\mathrm{d}\ln R^{\pm}/\mathrm{d}\ln\xi = (U \pm C)/(U \pm C - 1). \quad (11)$$

From this it follows that characteristics $R^{\pm}$ coincide with ξ lines exactly when $U \pm C = 1$ is fulfilled. These limiting characteristics play an important role with respect to causality in the flows to be discussed. They divide flow regions which are in causal contact with the gas at $r=0$, $t=0$ from those which are not. For times $t<0$ this is illustrated in Figure 1.

2.3. *Conservation of Mass and Entropy*

Inserting ansatz (2) and (3), the continuity equation in system (1) can be written in reduced differential form

$$\mathrm{d}U + (U-1)\,\mathrm{d}\ln G + (n+\varkappa)\,U\,\mathrm{d}\ln\xi = 0. \quad (12)$$

Dividing (12) by $(U-1)$ and taking into account (6), one obtains a complete differential with the integral

$$(1-U(\xi))\,G(\xi)\,R(\xi, a)^{n+\varkappa} = K_1(a) \quad (13)$$

for $U<1$ expressing conservation of mass. The constant K_1 is independent of ξ. The adiabatic integral $p/\varrho^{\gamma} = \varrho^{1-\gamma}c^2/\gamma = \text{const}$ expressing conservation of entropy along particle trajectories as long as no shock passes reduces to

$$(R^{\varkappa} G)^{1-\gamma}(\alpha(\xi/R)^{1/\alpha} R\,C)^2 = K_2(a). \quad (14)$$

The conservation laws (13) and (14) allow to express $G(\xi)$ and $R(\xi, a)$ as functions of $U(\xi)$ and $C(\xi)$ alone

$$G(\xi) = K_3(\alpha\,\xi^{1/\alpha}\,C(\xi))^{\mu(n+\varkappa)/\beta} (1-U(\xi))^{(\varkappa+\mu\lambda)/\beta}, \quad (15)$$

$$R(\xi, a) = K_4\,a(\alpha\,\xi^{1/\alpha}\,C(\xi))^{-\mu/\beta} (1-U(\xi))^{-1/\beta} \quad (16)$$

with $\mu = 2/(\gamma-1)$, $\beta = n - \mu\lambda$, $\lambda = 1/\alpha - 1$, and constants K_3 and K_4 which are independent of ξ and a. Notice that $R(\xi, a)/a$ has to be independent of a due to (8). These algebraic relations for density and particle trajectories reduce the mathematical problem to one of finding $U(\xi)$ and $C(\xi)$.

2.4. *The Reduced Differential Equation for U and C*

Complete selfsimilar reduction of system (1) by (2) and (3) and elimination of $\ln G$ by (12) gives finally the differential equations

$$a_1\,\mathrm{d}U + b_1\,\mathrm{d}C + d_1\,\mathrm{d}\ln\xi = 0,$$
$$a_2\,\mathrm{d}U + b_2\,\mathrm{d}C + d_2\,\mathrm{d}\ln\xi = 0 \quad (17)$$

with coefficients

$$a_1 = C/\mu, \quad b_1 = U-1,$$
$$a_2 = U-1, \quad b_2 = \mu C,$$
$$d_1 = C[\mathrm{U}(1+n/\mu) - 1/\alpha], \quad (18)$$
$$d_2 = U(U-1/\alpha) + C^2[\mu + (\varkappa+\mu\lambda)/(\gamma(1-U))],$$

where $\mu = 2/(\gamma-1)$, $\lambda = 1/\alpha - 1$. The remarkable feature of this reduction first noticed by Guderley is that the coefficients (18) depend, except for the fixed parameters n, γ, α, $\varkappa$, exclusively on the reduced velocities U and C, but not on space-time variables, r, t, ξ. This means that one has to solve a single ordinary differential equation

$$\mathrm{d}U/\mathrm{d}C = \Delta_1(U, C)/\Delta_2(U, C) \quad (19)$$

with the determinants

$$\Delta_1(U, C) = b_1 d_2 - d_1 b_2,$$
$$\Delta_2(U, C) = d_1 a_2 - a_1 d_2. \quad (20)$$

Explicit expressions for Δ_1 and Δ_2 are given in the appendix. Having solved (19) for appropriate boundary conditions to obtain $U(C)$, the function $C(\xi)$ follows from

$$\mathrm{d}\ln\xi/\mathrm{d}C = \Delta(U(C), C)/\Delta_2(U(C), C) \quad (21)$$

with

$$\Delta = a_1 b_2 - b_1 a_2 = C^2 - (1-U)^2 \quad (22)$$

by simple integration, and $U(\xi)$ correspondingly.

In general, (19) and (21) have to be solved numerically. Analytical solutions exist for a few important cases, and some of them will be presented in the following sections. A rather general overview over the solutions of (19) was given by Guderley in his 1942 paper, and his essential figure is reproduced here in Figure 2. It shows the solution curves in the U, C plane for a special parameter set: $n=3$, $\gamma=7/5$, $\alpha=0.75$, $\varkappa=0$. The arrows indicate the direction of increasing ξ. The selected sector of the U, C plane contains all the different solutions discussed below and provides a unifying picture. The plane is shown under central projection such that points U, C at infinity $U\to-\infty$, $C\to+\infty$ are mapped into the line P_6P_7; also coordinate lines $U=\text{const}$ intersect in P_6 and lines $C=\text{const}$ in P_7. The advantage of this mapping is that the important behaviour of the solutions at infinity are displayed

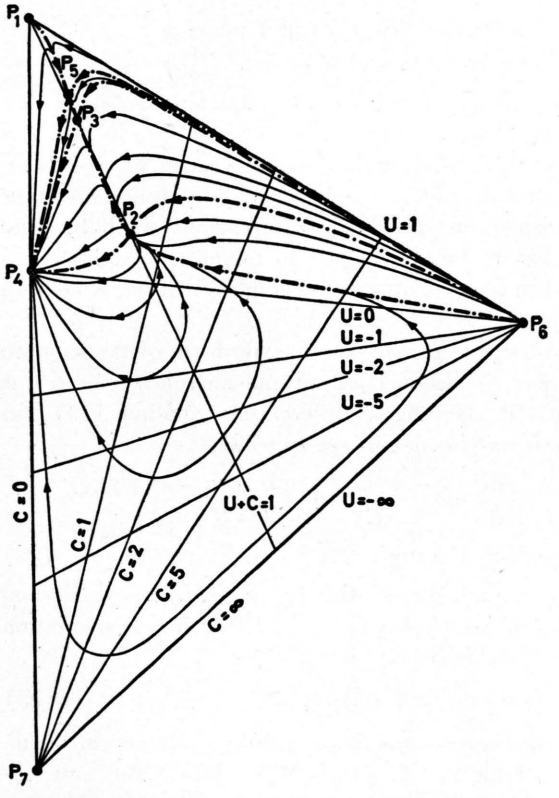

Fig. 2. Guderley's chart of solutions in the U, C plane for $n=3$, $\gamma=7/5$, $\alpha=0.75$ and $\varkappa=0$. Singular points are labelled by P_1 to P_7. Solid curves describe solutions of (19), dash-dotted curves are separatrices. The arrows give the direction of increasing ξ. A projection of the U, C plane has been chosen such that the behaviour of solutions at infinity is seen. The plot has been taken from [1].

explicitly. Solution curves $U(C)$ of (19) cannot intersect except at singular points where both determinants

$$\Delta_1(U,C)=0\,,\quad \Delta_2(U,C)=0 \tag{23}$$

vanish. In the U, C plane of Fig. 2 one finds seven singular points designated by P_1 to P_7 in Guderley's notation. The separatrices which connect the singular points and divide the U, C plane in subregions are plotted as dash-dotted lines. Another important line is given by $U+C=1$. On this line one has $\Delta=0$ and therefore

$$\mathrm{d}\ln\xi/\mathrm{d}C=0 \tag{24}$$

due to (21) and (22) except at the singular points P_1, P_2 and P_3 where also $\Delta_2=0$. Equation (24) implies that solutions $\xi(C)$ have an extremum when crossing the $U+C=1$ line, and no single-valued inversion $C(\xi)$ exists. Such solution curves are rejected as unphysical. Physical solutions have to cross at the singular points.

Important solutions are given predominantly by the separatrices. Examples are:

(1) the solitary separatrix P_6P_2 (the lower one in Fig. 2) representing central explosions and centrally reflected waves after implosion;

(2) the separatrices P_1P_5 and P_6P_5 representing cumulative implosions where all matter finally collapses into a point;

(3) the separatrix $P_4P_3P_6$ or $P_4P_3P_1$ (for different parameters γ, α) representing non-cumulative implosions of Guderleys's type.

Before going into the detailed description of the particular solutions, a brief characterisation of the singular points P_1 to P_7 is given.

2.5. The Singular Points and the Shock Line

The condition (23) for the singular points is that the determinants (20)

$$\Delta_1=b_1d_2-d_1b_2=0\,,$$
$$\Delta_2=d_1a_2-a_1d_2=0$$

vanish simultaneously. This is satisfied for

(1) $a_1=a_2=b_1=b_2=0\,,$ (P_1),

(2) $a_1/a_2=b_1/b_2=d_1/d_2\,,$ $(P_2 \text{ and } P_3)$,

(3) $d_1=d_2=0\,,$ $(P_4 \text{ and } P_5)$.

With the explicit form of the coefficients (18) one obtains the coordinates of the singular points.

Point P_1 is located at $U_1=1$, $C_1=0$. It satisfies the boundary conditions of a free surface, since it corresponds to a fixed gas element ($U=1$, compare (7)) with vanishing density ($G_1\to 0$ due to (15)) and vanishing pressure $p\sim G_1 C_1^2$.

Points P_2 *and* P_3 are located on the sonic line $U+C=1$ where $\Delta=a_1 b_2-b_1 a_2=0$. They correspond to limiting characteristics (compare (10)). Physical solution curves connecting flow regions $U+C>1$ with flow regions $U+C<1$ have to cross the sonic line through P_2 or P_3. These points exist only for a limited region of the parameter space. The quadratic equation to determine $U_{2,3}$ is discussed in the appendix.

Point P_4 is located at $U_4=0$, $C_4=0$. In the neighbourhood of this point (19) reduces to $\mathrm{d}U/\mathrm{d}C\cong U/C$ showing that it is a proper node point. Solution curves come in on straight lines with slopes given by the Mach number $M=U/C$. Equation (21) reduces to $\mathrm{d}\ln\xi/\mathrm{d}C\cong-\alpha/C$ with the integral

$$\xi\sim 1/C^{\alpha}\quad\text{for } C\to 0 \tag{25}$$

showing that P_4 corresponds to $\xi=\infty$ (assuming $\alpha>0$) and describes the flow for $r\to\infty$ at times $t\neq 0$ as well as for $t=0$ and $r>0$.

Point P_5 is located at

$$\begin{aligned} &U_5=(\mu/(n+\mu))\,(1/\alpha),\\ &C_5=U_5\cdot\sqrt{n}/\mu\quad\text{for isentropic flow }(\varepsilon=0),\\ &C_5=((n\gamma/\mu)U_5^2(1-U_5)/((n-2)U_5+\varkappa+2))^{1/2}\\ &\qquad\text{for non-isentropic flow }(\varepsilon\neq 0). \end{aligned} \tag{26}$$

Since $\Delta_2=0$, but $\Delta\neq 0$ for P_5 in general, one has $\mathrm{d}\ln\xi/\mathrm{d}C\to\pm\infty$ when approaching P_5 and ξ tends either to $+\infty$ or to 0. Therefore P_5 describes boundaries either far outside at $r\to\infty$ as point P_4 or in the centre at $r=0$.

Point P_6 is located at $C_6\to\infty$ and U_6 finite. Its analytic structure is investigated in the appendix. Solution curves enter either along the solitary separatrix (P_2P_6 in Fig. 2), which describes central explosions with diverging temperature in the centre $r\to 0$, or they approach the $U=1$ line (for $\varepsilon>0$) and describe non-isentropic imploding shells.

Point P_7, located at $U_6\to-\infty$ and C_6 finite, has no immediate physical significance and is only mentioned for completeness.

Shock point A. Shock discontinuities represent another important boundary situation, not described by singular points. A shock front moving on a ξ line, $R_s=\xi_s|t|^{\alpha}$, has the velocity $u_s=\alpha R_s/t$ or, in reduced form, $U_s=1$. This allows to express the jump relations at a shock front in terms of the reduced quantities as given in the appendix. For a strong shock running into a gas at rest, one obtains

$$\begin{aligned} &U_A=2/(\gamma+1),\\ &C_A=\sqrt{2\gamma(\gamma-1)}/(\gamma+1) \end{aligned} \tag{27}$$

for the velocities behind the shock.

When varying the parameters n, γ, α, $\varkappa$, the points P_2, P_3, P_5 and A change their position or become complex and disappear as points in the U, C plane. The singular points may also interchange their individual character (e. g. saddle, node) when meeting each other. No attempt is made in this paper to discuss all possible cases. However, various situations which are important for spherical implosions are exposed by the examples given below.

3. The Taylor-Sedov Point Explosion and Related Solutions

As a first example the explosion solution corresponding to the lower separatrix P_2P_6 in Fig. 2 is discussed. It describes strong central explosions in a uniform gas as well as centrally reflected waves which occur in spherical implosions. In both cases it has to be connecteed to an outer solution by a shock front. Different examples will be shown in Figs. 3 b, 5 b, 6 b and 7 b.

First, the general asymptotic form of the solution in the neighbourhood of the singular point P_6 is derived. The basic differential equation (19) has the form (for details see appendix)

$$\frac{\mathrm{d}U}{\mathrm{d}C}=\frac{(1-U)}{C}\cdot\frac{nU+(\varkappa-2\lambda)/\gamma}{1-U+\varepsilon/2\gamma}\quad\text{for } C\to\infty. \tag{28}$$

Apparently, the solution curves $U(C)$ approach constant U values for $C\to\infty$, either $U=1$, a solution discussed in Sect. 6, or

$$U=-(\varkappa-2\lambda)/n\gamma \tag{29}$$

which corresponds to the solitary solution curve approaching P_6. Inserting (29) into (21), one obtains $\mathrm{d}\ln\xi/\mathrm{d}\ln C=-1/(1+\varepsilon n/2\nu)$ with $\nu=(n\gamma+\varkappa-2\lambda)$ and the integral

$$\xi\sim C^{-1/(1+\varepsilon n/2\nu)} \tag{30}$$

which shows that $\xi\to 0$ for $C\to\infty$ when approaching P_6 on this line, provided that $\varepsilon n/2\nu>-1$ which

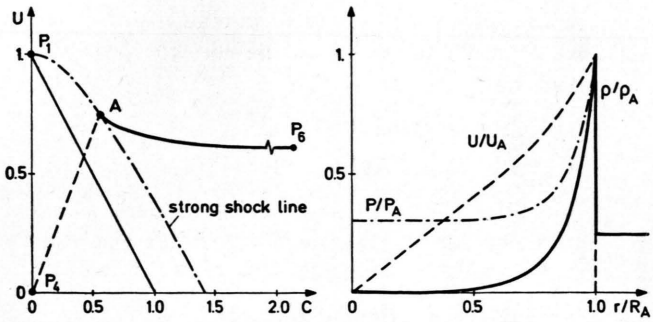

Fig. 3a. Taylor-Sedov solution for a strong point explosion in the U, C plane. Parameters: $n=3$, $\gamma=5/3$ $\alpha=2/5$, $\varkappa=0$.

Fig. 3b. Density ϱ, pressure p and velocity u of the Taylor-Sedov solution as a function of radius r. The label A denotes the values at the shock front.

is fulfilled for the cases studied here. It is therefore a solution which includes the centre $r=0$.

With (29) and (30), one obtains from (2) and (15) the expressions

$$\begin{aligned} u(r,t) &= -\alpha(\varkappa-2\lambda)/n\gamma(r/t), \\ \varrho(r,t) &\sim r^{n\varepsilon/\nu}\cdot t^{\alpha(\varkappa-n\varepsilon/\nu)}, \\ T(r,t) &\sim c^2 \sim r^{-n\varepsilon/\nu}\cdot t^{\alpha(n\varepsilon/\nu-2\lambda)}, \\ p(r,t) &\sim r^0\cdot t^{\alpha(\varkappa-2\lambda)} \end{aligned} \tag{31}$$

which describe the flow asymptotically for $r/t^\alpha \to 0$ and $t>0$. A characteristic feature of this solution is that the pressure $p\sim r^0$ is uniform in the centre, whereas the density $\varrho\sim r^{n\varepsilon/\nu}$ vanishes and the temperature $T\sim r^{-n\varepsilon/\nu}$ diverges in case that the entropy exponent is $\varepsilon>0$. For the definition of the various exponents compare (5).

For the special parameters $\alpha=2/5$, $\varkappa=0$, $n=3$, the present solution represents the famous solution of a strong point explosion in a uniform gas which has been discovered independently by Taylor [8] and Sedov [9]. It is shown explicitly for $\gamma=5/3$ in Figures 3 a and 3 b. Figure 3 a shows a part of the U, C plane with the solution curve coming from P_6 and terminating in the strong shock point A with coordinates given by (27). It corresponds to the shock trajectory $R_A=\xi_A t^{2/5}$. The dashed line AP_4 indicates the jump to the unperturbed gas ($U=C=0$) in front of the shock. It has been shown by Sedov that there exists a closed integral of (19) in this case $C^2=(\gamma(\gamma-1)/2)\cdot U^2(U-1)/(1-\gamma U)$ due to energy conservation, and the solution can be given completely in analytical form [11, 32]. Distributions of density, pressure and velocity are plotted in Figure 3 b.

Another interesting analytical situation is obtained for $\varkappa=2\lambda$. In this case, the lower separatrix P_2P_6 coincides with the $U=0$ axis, the gas in the centre is at rest and the relations (31) hold exactly. In particular the pressure is constant in space and time. This situation may occur as a result of a spherical implosion behind the centrally reflected shock and is of special interest for fusion applications. The isentropic case with $\varepsilon=\varkappa(\gamma-1)+2\lambda=0$ is discussed in Sect. 5 and the non-isentropic case with $\varepsilon>0$ in Section 6.

4. Kidder's Homogeneous Compression and Related Cumulative Solutions

In this section, it is shown that Kidder's solution for homogeneous isentropic implosions is represented by the separatrices P_6P_5 (full sphere implosion [3]) and P_1P_5 (hollow sphere implosion [4]) in Guderley's chart of solutions in Fig. 2, provided one chooses $\alpha=1/2$ and $\varkappa=-3$ in addition to $n=3$ and $\gamma=5/3$. Generalisations as discussed by Anisimov et al. [5] then follow for other values of α and $\varkappa$. With $\alpha=1/2$ and $\varkappa=-3$, the entropy exponent (5) is $\varepsilon=0$ and the corresponding flow is isentropic. According to (26), the singular point P_5 is located at

$$U_5=1, \quad C_5=1/\sqrt{3} \tag{32}$$

and the separatrix $P_1P_5P_6$ in the U, C plane falls into the $U=1$ axis as shown in Figure 4 a. This is easily checked from (18) – (20). In Sect. 2.2 it has been derived that particle trajectories $R(t,a)$ coincide with ξ lines for $U=1$, and therefore one has $\xi=R(t,a)/|t|^{1/2}=a/t_c^{1/2}$ where a is the particle's position at time $t=-t_c$, and one can write

$$R(t,a)=a\,h(t), \tag{33}$$

$$h(t)=(-t/t_c)^{1/2} \tag{34}$$

for $t<0$. Relation (33) defines homogeneous flow and already proves the equivalence with Kidder's solution. Its explicit form is obtained from (21)

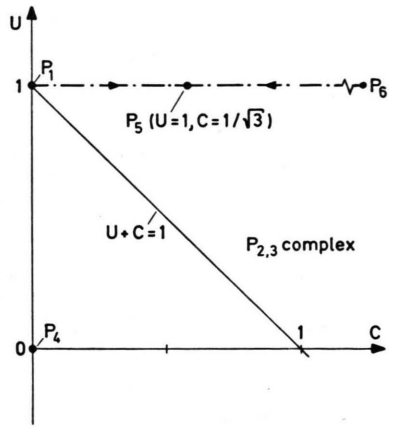

Fig. 4a. Kidder's solution for homogeneous compression in the U, C plane. Parameters: $n=3, \gamma=5/3, \alpha=1/2, \varkappa=-3$. Full sphere implosion is described by line P_6P_5, hollow sphere implosion by line P_1P_5. At P_5 one has $\xi=\infty$.

which for the present parameters and $U=1$ reduces to

$$\mathrm{d}\ln\xi/\mathrm{d}C = 3\,C/(1-3\,C^2) \tag{35}$$

and has the integral

$$C(\xi)^2 = (1+k\,\xi^2)/3\,k\,\xi^2\,, \tag{36}$$

where k is the integration constant. It is seen that $C\to 1/\sqrt{3}$ for $\xi\to\infty$, and P_5 is a $\xi=\infty$ point in this case describing the flow far outside at $r\to\infty$. The inner boundary $\xi=0$ is reached with $C\to\infty$ at P_6 for $k>0$, and in this case P_6P_5 describes a *full sphere*. For $c(a,t)=\alpha\,R(t,a)/t\cdot C(\xi)$ one obtains with $\alpha=1/2$, $\xi=a/t_c^{1/2}$ and (33), (34), and (36)

$$c^2(a,t) = c_0^2(1+\beta(a/R_a)^2)/h(t)^2\,, \tag{37}$$
$$c_0 = R_a/(2\,t_c\sqrt{3\,\beta}), \quad \beta = k\,R_a^2/t_c\,,$$

and R_a is the outer radius of the sphere at $t=-t_c$. The solution for the *hollow sphere* is obtained from (36) with $k<0$. The inner boundary is described by the singular point P_1 from where the solution curve starts with $C=0$ and a finite value of ξ and runs to P_5. Taking $k=-t_c/R_i^2$ and $c_0=c(R_a,-t_c)$ where R_i and R_a are inner and outer radius of the hollow sphere at time $t=-t_c$, respectively, one obtains from (36)

$$c^2(a,t) = c_0^2(a^2-R_i^2)/(R_a^2-R_i^2) \cdot 1/h(t)^2 \tag{38}$$

and the collapse time is related to the radii by

$$t_c = \sqrt{(R_a^2-R_i^2)/3}/(2\,c_0) \tag{39}$$

in this case. Isentropic flow implies $\varrho\sim c^{2/(\gamma-1)}$ and $p\sim c^{2\gamma/(\gamma-1)}$, and one has therefore for density and pressure

$$\varrho(a,t)/\varrho_0 = (c(a,t)/c_0)^3\,, \tag{40}$$
$$p(a,t)/p_0 = (c(a,t)/c_0)^5\,. \tag{41}$$

Equations (37) – (41) represent Kidder's solution. It is illustrated in Figure 4b. It holds also exactly for non-selfsimilar time evolution [3]

$$h(t) = (-t/t_c(1+t/4\,t_c))^{1/2}$$

which approaches selfsimilarity only for $t\to 0$.

Kidder's solution belongs to the cumulative implosions where all imploding matter finally collapses into the centre $r=0$. It is now shown that all solutions running into the singular point P_5 for $\xi\to\infty$ are cumulative. In the neighbourhood of P_5 one has

$$\mathrm{d}R/\mathrm{d}t \cong (\alpha\,R/t)\,U_5 \quad (\text{near } P_5) \tag{42}$$

with $U_5=\mu/(n+\mu)\cdot 1/\alpha$ from (26) and the integral

$$R(t,a) \sim |\,t\,|^{\mu/(n+\mu)}\,. \tag{43}$$

This means that all particle trajectories $R(t,a)\to 0$ for $t\to 0$, and the flow is cumulative.

Driving the gas by a piston which moves on one of the trajectories (43), say $R_a=R(t,a)$, the mechanical power of the piston acting on the gas is

$$P(t) \sim R_a^{n-1}\cdot p(R_a,t)\cdot u(R_a,t)\,. \tag{44}$$

With the pressure at the piston

$$p(R_a,t) \sim (c(R_a,t))^{\mu\gamma} \sim ((R_a/t)\,C_5)^{\mu\gamma}$$

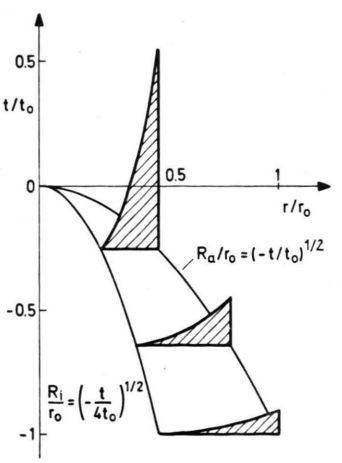

Fig. 4b. Kidder's solution a for collapsing hollow sphere in the r, t plane. Trajectories of the inner radius R_i and the outer radius R_a are shown. Density distributions $\varrho(r,t)$ have been inserted as shaded areas at three times; the vertical extension of these areas gives the density.

the piston velocity

$$u(R_a, t) \sim (R_a/t)\, U_5$$

and (43) one derives from (44) the general law for the piston power [5]

$$P(t) \sim |t|^{-(3n+\mu)/(n+\mu)}. \tag{45}$$

One should notice that relations (43) and (45) hold for flows near P_5 and times $t \to 0$ for any n and $\mu = 2/(\gamma - 1)$ and are independent of α and $\varkappa$. Taking the spherical case $n = 3$ and a $\gamma = 5/3$ gas one obtains from (43)

$$R(t, a) \sim |t|^{1/2} \tag{43 a}$$

showing that asymptotically for $t \to 0$ Kidder's trajectories (33), (34) hold for any P_5 flow, and the corresponding power law (45) of the piston is

$$P(t) \sim 1/|t|^2. \tag{45 a}$$

This is the power law which has been found for optimal isentropic compression of ICF targets by Nuckolls et al. [2] from a series of numerical implosion runs. Here it follows as a general law for cumulative flows with $n = 3$ and $\gamma = 5/3$. As we shall see in the next section it holds also approximately for non-cumulative flows for which the solution curve passes close to P_5.

It is apparent from Guderley's chart in Fig. 2 that generalized cumulative solutions of Kidder's type exist for parameters α, $\varkappa$ chosen such that $U_5 + C_5 > 1$ and $U_5 \leqq 1$. They may be isentropic or non-isentropic. In addition to the implosions discussed above, there are also solutions with a strong shock at the inner front running into undisturbed gas. They correspond to solution curves connecting P_5 with the strong shock point A. All these cases have been discussed in the context of ICF target implosions by Anisimov and Inogamov [5].

5. Uniform Gas Compression

In this section, selfsimilar compression of an initially uniform, isentropic gas sphere into a finally uniform, isentropic gas sphere of arbitrarily high density is described. It corresponds to solution curves connecting the singular points P_2 and P_4 for $t < 0$, and to curves in the lower part of the U, C plane which are connected to the final uniform gas by a shock front, for $t > 0$. The curves are shown for $\alpha = 1$ and $\varkappa = 0$ in Figure 5 a. Compare also Figure 2. An illustration of how the gas elements move and how the density distribution evolves during compression is given in Figure 5 b. These solutions have been investigated by Ferro Fontan et al. [6] and by Rodriguez and Linan [7] and are discussed in some detail below.

The initial and final gas is at rest and corresponds to points on the $U = 0$ axis. For the uniform gas one has $\varkappa = 0$, and isentropic compression with $\varepsilon = \varkappa(\gamma - 1) + 2(1/\alpha - 1) = 0$ then requires $\alpha = 1$. For these parameters, the singular point P_2 has moved to $U_2 = 0$, $C_2 = 1$ and serves as boundary point at the inner front of the compression wave. Since P_2 is a node point, a whole bundle of physical solution curves starts from P_2. They correspond to different degrees of final compression ϱ_c/ϱ_0. Four of them are shown in Figure 5 a. The limiting curve d is given by the separatrix $P_2P_5P_4$. Since it contains P_5, it is a cumulative solution with infinite compression. In contrast to Kidder's case in Sect. 4, however, P_5 has now moved from the region $U + C > 1$ into region $U + C < 1$ and has changed from a node point into a saddle point when crossing $U + C = 1$. The curves a, b, c neighbouring d therefore do not run into P_5, but turn around and move to the $\xi = \infty$ point P_4. The closer they approach P_5, the higher is the compression during this initial phase with $t < 0$. For $t = 0$ ($\xi = \infty$) when the compression wave has reached the centre, the state of the gas is uniform with a uniform velocity inwards, as given by (4). Selfsimilar flows containing the singular point P_4 can be continued from times $t < 0$ to times $t > 0$. This was first discovered by Guderley [1]. Having in mind $u(r, t) = (\alpha\, r/t)\, U(\xi)$, the sign of U has to change when the sign of t changes. The solution curves therefore continue for $t > 0$ in the lower half of the U, C plane. In the neighbourhood of P_4 which corresponds to regions $r \to \infty$ the curves have the same Mach number $M = U/C$ as the ones for $t < 0$. However, in the central region $r \to 0$, the imploding flow is now disrupted by an outgoing shock and the flow behind this shock is described by the separatrix P_6P_2 which has been discussed already in Section 3. For the present parameters $\alpha = 1$ and $\varkappa = 0$, the central solution is simply a uniform gas. The location of the shock jump S_1S_2 in Fig. 5 a is determined by the general shock conditions (A 8) and (A 9) given in the appendix.

The separation into two flow regions connected by a shock is clearly seen in the density distribution the shock is constant in space and time. The shock

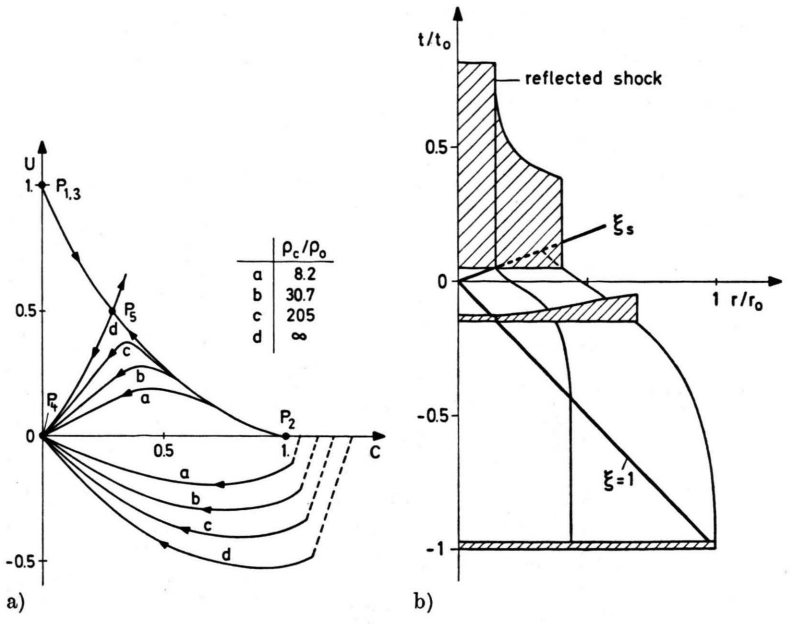

Fig. 5a. Solutions in the U, C plane describing compression of a uniform gas into a uniform gas at higher density. Parameters: $n=3$, $\gamma=5/3$, $\alpha=1$, $\varkappa=0$. The curves a, b, c and d correspond to different ratios between the final density ϱ_c and the initial density ϱ_0.

Fig. 5b. Solution b of Fig. 5a in the r, t plane. The front trajectory ($\xi=1$) of the compression wave for $t<0$ and the trajectory of the reflected shock ($\xi=\xi_s$) for $t>0$ as well as two particle trajectories are shown. Density distributions have been inserted as shaded areas for the initial unperturbed gas, for a time $t<0$ when the wave is travelling inwards and for a time $t>0$ with the constant gas in the centre and still imploding gas in front of the reflected shock. A uniform, vertical density scale has been chosen.

for $t>0$ in Figure 5 b. The gas in the centre behind is weak and has constant strength. The entropy of each incoming gas element is raised by the same amount so that the gas is transformed from one isentropic state into another. Actually, the entropy increase is very small. An upper limit is given by case d. One obtains numerically for the shock strength $S=p_2/p_1=1.96$, for the density jump $\varrho_2/\varrho_1=1.48$ and for $A_2/A_1=1.016$ in this case. Here, $A=p/\varrho^\gamma$ and the indices 1 and 2 refer to the gas in front of and behind the shock, respectively. The density ratio between the final state and the constant state at $t=0$ is $\varrho_c/\varrho(t=0)=5.90$ in the limit d. It should be understood that the major part of the compression is achieved in the period $t<0$ when the solution curve passes close to point P_5.

The closer this passage near P_5 is, the more the present solution approaches the cumulative flow described in Section 4. This includes that during the period of maximum compression at intermediate times $-1<t/t_0<0$ particle trajectories approximately follow parabolas $R(t,a)\sim|t|^{1/2}$ as derived in (43 a). This behaviour is seen in Figure 5 b. During this intermediate period also the piston power follows $P(t)\sim 1/|t|^2$ as given in (45 a). However, the present selfsimilar flow behaves more smoothly at the start ($t/t_0=-1$, flow near P_2) to avoid shock generation and at the end ($t/t_0\cong 0$, flow near P_4) to avoid total collapse. Here, we add that the problem of completely adiabatic compression of a constant gas into a compressed constant gas which avoids the reflected shock has been treated numerically by Morreeuw and Saillard [34] using characteristics. Their solution is of course non-selfsimilar.

Concerning ICF target implosions, pulse shapes with $P(t)\sim 1/|t|^2$ behaviour are difficult to achieve with existing drivers. Also compression to a finally uniform gas is not an optimal situation for ICF applications. A non-isentropic final configuration with a high temperature region in the centre is preferable. A selfsimilar implosion with such properties will be discussed in the next section.

6. Guderley's Imploding Shock Wave and the Non-isentropic Collapsing Hollow Sphere

As a last case, Guderley's solution for a spherically imploding shock wave [1] is discussed and how it can be generalised to describe a non-isentropic collapsing hollow sphere leading to arbitrarily high compression with diverging temperature in the centre of the compressed gas [35].

The imploding shock solution is shown in Figs. 6 a and 6 b. For times $t<0$, it connects the shock point A with the $\xi=\infty$ point P_4 by passing the sonic line $U+C=1$ through point P_3. For given parameters $n=3$, $\gamma=5/3$ and $\varkappa=0$, this solution exists only for a single value $\alpha=0.688$ and is uniquelly determined. Exponents α for other values of γ are found in Refs. [25 – 27]. The solution for

$t>0$ describing the flow after shock collapse in the centre is constructed in the same way as in Sect. 5 for the case of uniform gas compression. In Fig. 6 a

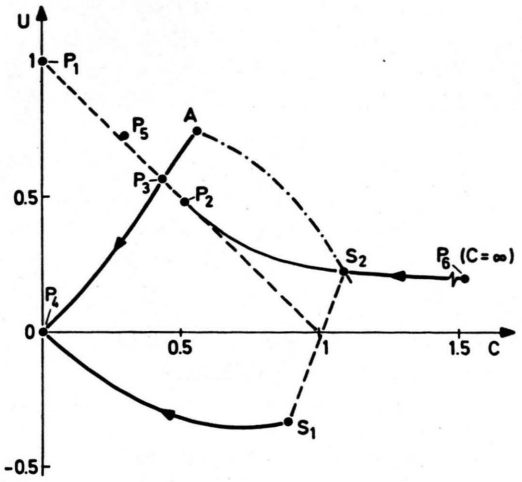

Fig. 6a. Guderley's imploding shock solution in the U, C plane. It corresponds to AP_3P_4 for $t>0$ and to $P_4S_1S_2P_6$ for $t>0$. Points on the dash-dotted line AS_2 can be reached from points on P_4S_1 by shocks. Parameters are $n=3$, $\gamma=5/3$, $\alpha=0.688$ and $\varkappa=0$. More details are given in the text.

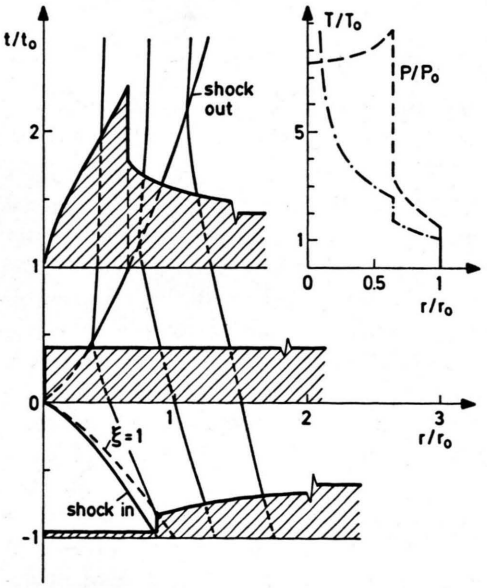

Fig. 6b. The solution of Fig. 6a in the r, t plane. Trajectories are plotted for ingoing and outgoing shock as well for three gas elements. The broken line ($\xi=1$) is the limiting characteristic. Density profiles before, at and after collapse are shown as shaded areas with a uniform vertical density scale. Distributions of pressure and temperature behind the reflected shock are shown in the insert in units p_0 and T_0 which are the values at $r=r_0$ and $t=0$.

it consists of the line P_4S_1 for the outer flow region and the line S_2P_6 for the central flow region with the shock S_1S_2 connecting both regions. The dash-dotted line AS_2 represents gas states behind the shock which may be reached from points on P_4S_1 by the general shock relations (A 8) and (A 9) which are given in the appendix.

Trajectories of the ingoing and outgoing (reflected) shock front and three particle trajectories as well as three density profiles (inserted shaded areas) are shown in the r, t diagram in Figure 6 b. For large radii the densities converge to a finite value which is indicated at the right end of each profile. This value is independent of time and 9.47 times larger than the density ϱ_0 of the unperturbed gas for the present parameters. The gas is compressed 4 times at the shock front and the additional density increase is due to adiabatic compression. At collapse time $t=0$, the density is uniform, although velocity, pressure, etc. are not as one may check from (4). The Mach number is $M_0=0.956$ and the entropy exponent $\varepsilon=0.907$. For times $t>0$, the reflected shock is travelling outwards and the state of the gas in the centre behind the shock is approximately described by (31). The density vanishes in the centre due to $\varepsilon>0$ and rises to a value of 32.0 ϱ_0 behind the shock front. This is the maximum density in Guderley's solution for $\gamma=5/3$ and stays constant with the shock running outwards. Higher compression cannot be reached by a selfsimilar shock wave imploding in a $\gamma=5/3$ gas. The reason is that the gas is strongly heated by the shock. This prevents further compression. The maximum compression, however, is a function of γ and increases without limit for $\gamma\to 1$ (see [25, 26]). Distributions of temperature T and pressure P at $t/t_0=1$ are shown in the insert in the upper right corner of Figure 6 b. The temperature diverges for $r\to 0$, whereas the pressure is almost uniform in the centre and rises slightly towards the shock front. The gas velocity behind the shock is directed outwards, whereas the gas in front of the shock is still flowing inwards.

We now turn to the case of a non-isentropic imploding hollow sphere. As it is shown in Fig. 7 a, it corresponds to the same solution curve in the U, C plane as the imploding shock wave described above except that now the condition to hit the shock boundary point A is dropped and the separatrix P_4P_3 is followed up to the node point P_6. Such solution curves exist for a broad range of parameters α

and $\varkappa$ as long as P_3 exists and $\varepsilon > 0$. The plotted solution corresponds to $\alpha = 0.7$ and $\varkappa = 3$ again with $n = 3$ and $\gamma = 5/3$. Here, the important new feature

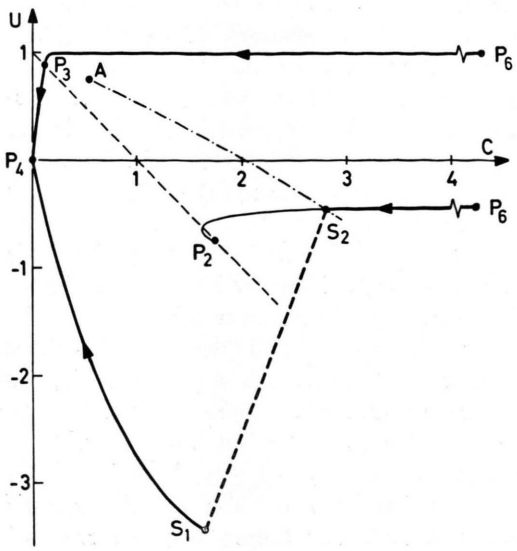

Fig. 7a. Generalised Guderley solution in the U, C plane describing non-isentropic imploding hollow spheres. Compare caption of Figure 6a. Parameters are $n = 3$, $\gamma = 5/3$, $\alpha = 0.7$ and $\varkappa = 3$ implying $\varepsilon = 20/7$.

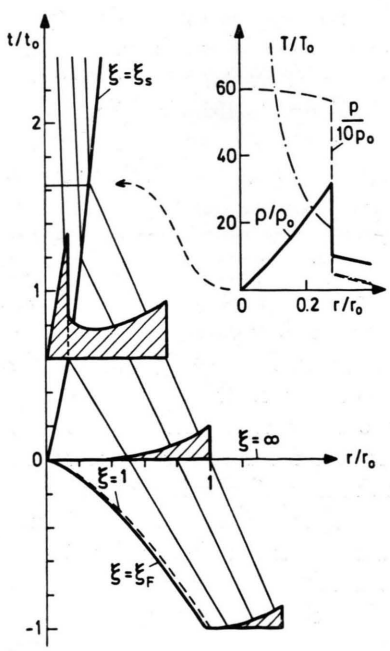

Fig. 7b. The hollow sphere implosion of Fig. 7a in the r, t plane. For details see caption of Figure 6b. The solid line $\xi = \xi_F$ gives the trajectory of the inner surface. Temperature and entropy diverge at this surface.

is the density exponent $\varkappa > 0$. It implies density distributions which are sloping towards the inner surface as shown in Figure 7 b. Such density profiles typically occur in ICF target implosions. The continuation of these solutions to times $t > 0$ is obtained in the same way as above for shock implosion. However, it turns out that depending on α and $\varkappa$ arbitrarily high compression can be achieved in the present case.

It has still to be shown that P_6 when approached along $U = 1$ (see Fig. 2 and Fig. 7 a) describes the inner surface of a hollow sphere. From (28) one finds $\mathrm{d}\ln|1-U|/\mathrm{d}\ln C \cong -2\nu/\varepsilon$ and the integral

$$C = C_F (1-U)^{-\varepsilon/2\nu} \tag{46}$$

for $U \to 1$, $C \to \infty$. The ξ dependence near P_6 follows from $\mathrm{d}U/\mathrm{d}\ln\xi \cong -\nu/\gamma$ and gives

$$\xi = \xi_F \exp((1-U)\gamma/\nu) \tag{47}$$

for $U \to 1$. Here, $C_F > 0$ and $\xi_F > 0$ are integration constants, ε and ν are defined by (5). A more detailed derivation of (46) and (47) is given in the appendix. It is seen that the solution curves approach $U = 1$ for $C \to \infty$ if $\varepsilon/2\nu > 0$ and that $\xi \to \xi_F > 0$ at P_6 indicating that P_6 describes an inner front. From (15) one obtains with Eqs. (46) and (47)

$$G(\xi) \sim 1/C(\xi)^2 \tag{48}$$

showing that the density $\varrho = r^\varkappa G$ vanishes at P_6, whereas the temperature $T \sim C^2 \to \infty$ diverges. A peculiar point is that the pressure does not vanish at P_6, but tends to a finite value $p \sim C^2 G \to p_F > 0$ at the front. Therefore the present solution does not satisfy the pressure boundary condition of a free surface. In fact, a free surface with diverging entropy will move in a non-selfsimilar way. Also, the gasdynamical description becomes invalid at such a front in general. Nevertheless, it is argued that the present selfsimilar solution represents an approximation to the actual gas flow in the sense of intermediate asymptotics [13]. A similar situation occurs in the problem of impulsive load on a plane surface where temperature and entropy diverge at the vacuum – gas interface. In the book of Zeldovich and Raizer [10] this case is studied in detail showing that the motion of the free surface is always non-selfsimilar, but that the flow at some distance behind the front approaches the selfsimilar solution rapidly. In the present case it has been checked that the front pressure of the selfsimilar solution is

small as compared to typical pressures inside the imploding shell [35] and that it tends to zero $p_F \sim (-t)^{\alpha(\varkappa-2\lambda)} \to 0$ for $(-t) \to 0$ provided that $\varkappa > 2\lambda$. This indicates that the present solution represents a valuable approximation, at least for $\varkappa > 2\lambda$, a situation which is typically found in ICF target implosions of initially shocked hollow spheres [36]. For $\varkappa \leqq 2\lambda$, a careful comparison with non-selfsimilar solutions would be necessary to substantiate the conjecture of intermediate asymptotics.

The evolution of density distribution in time as well as some particle trajectories are shown in Figure 7 b. It is important to observe that the gas elements implode with almost constant velocity, like freely flying matter. The front moves along $R_F = \xi_F |t|^{0.7}$. The broken line $\xi = 1$ is the limiting characteristic corresponding to the singular point P_3 in the U, C plane. Concerning the limiting characteristic, compare the discussion in Sects. 2.2 and 2.5. At time $t = 0$, the gas state is given by the power laws of (4); for the present parameters one has $\varrho = \varrho_0 r^3$ and the Mach number $M_0 = 7.09$. Due to the density slope the flow develops somewhat differently from Guderley's case in Fig. 6 b for times $t > 0$. The outgoing shock moves much slower, and the flow behind the shock is still directed inwards further compressing the gas. This situation occurs for $\varkappa > 2\lambda$. Distributions of density, temperature and pressure are shown as insert in the upper right corner of Fig. 7 b and should be compared with Figures 3 b and 6 b. Since $\varepsilon > 0$, the temperature diverges in the centre. The final compression of gas elements between time $t = 0$ ($\xi = \infty$) and time $t = t_s$ ($\xi = \xi_s$) when the reflected shock has just passed is the same for each gas element due to (9). Numerically it turns out that this final compression ratio is approximately a function of Mach number M_0 alone and satisfies $\varrho_s/\varrho_0 \cong 2.4\, M_0^{3/2}$. The corresponding relation for final pressure increase is $p_s/p_0 \cong 3.6\, M_0^3$ (see Ref. [35]).

The formation of a hot region in the centre of the compressed gas is important for DT ignition in ICF target implosions [36]. This requires an entropy distribution increasing inwards as described by $\varepsilon > 0$. From the present solution one learns that in single shell target implosions such an entropy distribution is not produced by the reflected shock. The reflected shock has constant strength (compare Sect. 5), and its effect is only to raise the entropy of each incoming gas element by the same amount. The entropy profile with $\varepsilon > 0$ has to be generated before void closure ($t = 0$). We mention that this is achieved in ICF applications by initial shocks typically passing the target shell as a consequence of beam switch on. They produce increasing entropy towards the inner surface when running through sloping density profiles, e. g. a rarefaction wave [36]. This latter process is also described by a plane selfsimilar solution of Guderley's shock type [20].

7. Summary and Concluding Remarks

The different branches of selfsimilar compression waves have been described with regard to applications for inertial confinement fusion. The unifying viewpoint has been adopted from Guderley's original work on imploding shock waves. The general solution depends on four parameters:

1. the dimensionality n (for spherical waves $n = 3$),
2. the adiabatic gas exponent γ (for a monoatomic gas $\gamma = 5/3$),
3. the selfsimilarity exponent α,
4. the density exponent $\varkappa$.

The character of a particular flow is determined by the singular points P_1 to P_6 which are passed by the solution curve. They are shown on Guderley's chart of solutions in Fig. 2 for a special set of parameters. The points P_4, P_5 and P_6 are of particular importance for imploding spheres and ICF applications. Points P_4 and P_5 correspond to $\xi = \infty$ and describe the flow at collapse time $t = 0$. Point P_6 describes the gas in the centre after collapse, i. e. the configuration in which fuel ignition and burn has to be achieved in ICF target implosions. In the following, essential features are summarised.

Cumulative flows in which a finite amount of matter is adiabatically compressed into a point are described by P_5. Adiabatic compression to very high densities is crucial for fuel confinement in ICF applications. The cumulative solutions (e. g. Kidder's homogeneous compression) are basic for understanding this process. As an important general result it is found that trajectories of cumulative flow are given by $R(t, a) \sim |t|^{\mu/(n+\mu)}$ with $\mu = 2/(\gamma - 1)$ and that the driving power has to follow the singular pulse shape $P(t) \sim |t|^{-(3n+\mu)/(n+\mu)}$ asymptotically for $t \to 0$.

Non-cumulative selfsimilar flows are obtained when the solution curve passes P_4. The unique feature of point P_4 is that it allows to connect solutions before collapse ($t<0$) to solutions after collapse ($t>0$). At time $t=0$ the wave front reaches the centre. For $t>0$ the solution contains an outgoing shock which is generated by wave reflection in the centre. It separates the flow into an inner gas region behind the reflected shock and an outer gas region which is still imploding.

The gas state in the centre behind the reflected shock is governed by P_6. Equation (31) gives the general asymptotic solution near point P_6. Outstanding features of combined P_4, P_6 flows (e. g. the uniform gas compression in Sect. 5, Guderley's shock wave and the non-isentropic hollow sphere implosion in Sect. 6) are:

(a) almost constant implosion velocity of individual gas elements;

(b) uniform Mach number at collapse time $t=0$ which may be used to characterise the imploding wave, e. g. Guderley's shock wave has $M_0=0.956$ for $n=3$, $\gamma=5/3$;

(c) constant strength of the reflected shock which implies that the entropy distribution over the incoming gas elements is not changed by the shock (except for adding a constant);

(d) approximately uniform pressure behind the reflected shock which is an important property for estimating energy gain of ICF targets [33] in a general way;

(e) a velocity field $u(r,t)\cong[-\alpha(\varkappa-2\lambda)/(n\gamma)]r/t$ in the centre for $t>0$ with the gas contracting for $\varkappa>2\lambda$, expanding for $\varkappa<2\lambda$ and at rest for $\varkappa=2\lambda$; the parameter combination $(\varkappa-2\lambda)$, where $\lambda=(1/\alpha-1)$, is determined by the pressure distribution $p=p_0 r^{\varkappa-2\lambda}$ at $t=0$;

(f) diverging temperature $T(r,t)\sim r^{-n\varepsilon/\nu}$ in the centre behind the reflected shock for $\varepsilon>0$ where $\varepsilon=\varkappa(\gamma-1)+2\lambda$ and $\nu=n\gamma+\varkappa-2\lambda$ (for cases of interest $\nu>0$); the exponent ε is determined by the entropy distribution of the imploding gas, $p/\varrho^\gamma\sim r^{-\varepsilon}$ at $t=0$.

Result (f) is important for understanding ignition in simple ICF targets. It says that the entropy profile required to form the hot ignition region in the centre of the gas has to be generated before collapse during implosion and therefore depends critically on driver pulse shape and initial shocks [36]. All results (a) – (f) are observed, at least qualitatively, in numerical ICF target calculations.

It is concluded that considerable qualitative insight into the gas dynamics of spherical implosions is obtained from the selfsimilar solutions which have been studied in this paper. The question, however, of how the present results are related to general non-selfsimilar implosions in a quantitative sense and to which extent and under which conditions they meet with Barenblatt's conjecture of "intermediate asymptotics" is not yet answered. It is our feeling that these fundamental aspects of inertial confinement fusion have still to be studied in more detail and that the selfsimilar solutions presented here will form the basis for a deeper understanding of the gasdynamical aspects.

Appendix

The explicit form of the determinants Δ_1 and Δ_2 obtained by inserting the coefficients (18) into (20)

$$\Delta_1=U(1-U)\left(\frac{1}{\alpha}-U\right)-C^2[nU+(\varkappa-2\lambda)/\gamma], \tag{A 1}$$

$$\Delta_2=C\left[(1-U)\left(\frac{1}{\alpha}-U\right)+U(\lambda+(n-1)\cdot(U-1))/\mu-C^2+\frac{\varepsilon}{2\gamma}\cdot\frac{C^2}{(U-1)}\right]. \tag{A 2}$$

The location of the singular points P_2 and P_3 is determined by the quadratic equation

$$(n-1)\gamma U^2+[\varkappa-2\lambda-\gamma(n-1-\lambda)]U-(\varkappa-2\lambda)=0 \tag{A 3}$$

giving $U_{2,3}$ and $C_{2,3}=1-U_{2,3}$. Equation (A 3) follows from $\Delta_1(U,C)=0$ setting $C=1-U$. It has real solutions for

$$(\gamma(n-1-\lambda)-(\varkappa-2\lambda))^2\geqq-4\gamma(n-1)(\varkappa-2\lambda). \tag{A 4}$$

Next, the point P_6 at $C\to\infty$ and U finite is shown to be a singular point at infinity. The leading terms of Δ_1 and Δ_2 for $C\to\infty$ are

$$\Delta_1\cong-C^2[nU+(\varkappa-2\lambda)/\gamma], \tag{A 5}$$

$$\Delta_2\cong-C^3[1+\varepsilon/(2\gamma(1-U))]. \tag{A 6}$$

Transforming P_6 with the help of

$$S = 1/C, \quad M = U/C$$

into P_6' at $S = 0$, $M = 0$, the differential equation (19) is transformed into

$$\frac{dM}{dS} = \frac{M}{S} - \frac{M n + S(\varkappa - 2\lambda)/\gamma}{S(1 + \varepsilon/(2\gamma(1 - M/S)))} \quad (A\,7)$$

using (A 5) and (A 6). Equation (A 7) has the structure $dM/dS = 0/0$ at P_6'. This identifies P_6 as a singular point. With expressions (A 5) and (A 6) one obtains

$$\frac{dU}{dC} \cong \frac{1-U}{C} \frac{n U + (\varkappa - 2\lambda)/\gamma}{1 - U + \varepsilon/2\gamma}$$

which may be written for $U \to 1$ in the form

$$\frac{d \ln |1-U|}{d \ln C} \cong - \frac{n + (\varkappa - 2\lambda)/\gamma}{\varepsilon/2\gamma} = - \frac{2\nu}{\varepsilon}$$

leading to the integral (46) for the solution curves $C(U)$ near P_6. For the ξ dependence one has

$$\frac{dU}{d \ln \xi} \cong - \frac{C^2[n U + (\varkappa - 2\lambda)/\gamma]}{C^2 - (1-U)^2} \cong - \frac{\nu}{\gamma}$$

leading to (47).

The general jump conditions [37] at a shock discontinuity, which map the state U_1, C_1 in front of the shock into the state U_2, C_2 behind the shock, are given for the reduced quantities

$$U_2 = 1 - \left[\frac{\gamma - 1}{\gamma + 1} + \frac{2}{\gamma + 1}\left(\frac{C_1}{1 - U_1}\right)^2\right](1 - U_1), \quad (A\,8)$$

$$C_2^2 = \frac{2\gamma(\gamma - 1)}{(\gamma + 1)^2}(1 - U_1)^2 + \left[1 - 2\left(\frac{\gamma - 1}{\gamma + 1}\right)^2 - 2\frac{\gamma - 1}{(\gamma + 1)^2}\left(\frac{C_1}{1 - U_1}\right)^2\right] C_1^2. \quad (A\,9)$$

The density jump follows then from

$$G_2/G_1 = (1 - U_1)/(1 - U_2). \quad (A\,10)$$

[1] G. Guderley, Luftfahrtforschung **19**, 302 (1942).
[2] J. Nuckolls, L. Wood, A. Thiessen, and G. Zimmermann, Nature **239**, 139 (1972).
[3] R. E. Kidder, Nucl. Fusion **14**, 53 (1974).
[4] R. E. Kidder, Nucl. Fusion **16**, 3 (1976).
[5] S. I. Anisimov and N. A. Inogamov, Zurnal Prikl. Mech. Techn. Fiz. **4**, 20 (1980), and Pisma Z. Techn. Fiz. **3**, 1112 (1977).
[6] C. Ferro Fontan, J. Gratton, and R. Gratton, Phys. Lett. **55 A**, 35 (1975) and Nucl. Fus. **17**, 135 (1977).
[7] M. Rodriguez and A. Linan, Selfsimilar Isentropic Implosions, preprint E.T.S.I. Aeronáuticos, Universidad Politécnica de Madrid, Madrid, Spain, 1980, and submitted to J. Fluid Mech. (1980).
[8] G. I. Taylor, Proc. Roy. Soc. London **A 201**, 159 and 175 (1950).
[9] L. I. Sedov, Prikl. Mat. Mekh. **10**(2), 241 (1946).
[10] Ya. B. Zeldovich and Yu. P. Raizer, Physics of Shock Waves and High Temperature Hydrodynamic Phenomena, Vol. II, Academic Press, New York 1967.
[11] L. I. Sedov, Similarity and Dimensional Methods in Mechanics, Academic Press, New York 1959.
[12] K. P. Stanyukovich, Unsteady Motion of Continuous Media, Pergamon Press, New York 1960.
[13] G. I. Barenblatt, Similarity, Selfsimilarity, and Intermediate Asymptotics, Consultants Bureau, New York 1979.
[14] R. Courant and K. O. Friedrichs, Supersonic Flow and Shock Waves, Interscience, New York 1948.
[15] C. F. v. Weizsäcker, Z. Naturforsch. **9a**, 269 (1954).
[16] W. Häfele, Z. Naturforsch. **10a**, 1006 (1955).
[17] W. Häfele, Z. Naturforsch. **10a**, 1017 (1955).
[18] S. v. Hoerner, Z. Naturforsch. **10a**, 687 (1955).
[19] F. Meyer, Z. Naturforsch. **10a**, 693 (1955).
[20] A. Sakurai, Commun. Pure Appl. Math. **13**, 353 (1960).
[21] C. Hunter, J. Fluid Mech. 8, 241 (1960).
[22] G. B. Whitham, Linear and Nonlinear Waves, John Wiley, London 1974, and J. Fluid Mech. **4**, 337 (1958).
[23] S. S. Jha and L. K. Chavda, Phys. Rev. **15 A**, 1289 (1976).
[24] J. Fujimoto and E. A. Mishkin, Phys. Fluids **21**, 1933 (1978).
[25] R. B. Lazarus and R. D. Richtmeyer, Report LA-6823-MS, Los Alamos Sc. Lab., 1977.
[26] M. Rodriguez and A. Linan, Report J.E.N. 405, Junta de Energia Nuclear, Madrid 1978.
[27] K. V. Brushlinski and Ya. M. Kazhdan, Uspekhi Mat. Nauk. **18** (2), 3 (1963).
[28] I. B. Bernstein and D. L. Book, Astrophys. J. **225**, 633 (1978).
[29] I. B. Bernstein and D. L. Book, Astrophys. J. **240**, 223 (1980).
[30] D. L. Book and I. B. Bernstein, J. Plasma Physics **23**, 521 (1980).
[31] K. V. Brushlinski, preprint "On the stability of an imploding spherical shock wave" (in Russian), No. 81, Keldysh Institute for Appl. Mathematics, Moscow 1980.
[32] R. E. Kidder, Nucl. Fusion **16**, 405 (1976).
[33] J. Meyer-ter-Vehn, Nucl. Fusion **22**, 561 (1982).
[34] J. P. Morreeuw and J. Saillard, Nucl. Fusion **18**,1263 (1978).
[35] J. Meyer-ter-Vehn and C. Schalk, submitted to Nucl. Fusion (1982).
[36] J. Meyer-ter-Vehn and N. Metzler, Target Design for Heavy Ion Beam Fusion, Report MPQ 48, Max-Planck-Institut für Quantenoptik, Garching (FRG) 1981.
[37] L. D. Landau and E. M. Lifshitz, Fluid Mechanics, Pergamon Press, Oxford 1959.

Verantwortlich für den Inhalt: A. KLEMM
Satz und Druck: Konrad Triltsch, Würzburg